Available online at www.sciencedirect.com

ScienceDirect

Advances in Space Research 61 (2018) 1702–1716

ADVANCES IN SPACE RESEARCH (a COSPAR publication)

www.elsevier.com/locate/asr

Case study of inclined sporadic E layers in the Earth's ionosphere observed by CHAMP/GPS radio occultations: Coupling between the tilted plasma layers and internal waves

Vladimir N. Gubenko [a,*], A.G. Pavelyev [a], I.A. Kirillovich [a], Y.-A. Liou [b]

[a] Kotel'nikov Institute of Radio Engineering and Electronics of the RAS, Fryazino, Moscow Region, Russia
[b] Center for Space and Remote Sensing Research, National Central University, Chung-Li, Taiwan

Received 31 March 2017; received in revised form 26 September 2017; accepted 4 October 2017
Available online 13 October 2017

Abstract

We have used the radio occultation (RO) satellite data CHAMP/GPS (Challenging Minisatellite Payload/Global Positioning System) for studying the ionosphere of the Earth. A method for deriving the parameters of ionospheric structures is based upon an analysis of the RO signal variations in the phase path and intensity. This method allows one to estimate the spatial displacement of a plasma layer with respect to the ray perigee, and to determine the layer inclination and height correction values. In this paper, we focus on the case study of inclined sporadic E (E_s) layers in the high-latitude ionosphere based on available CHAMP RO data. Assuming that the internal gravity waves (IGWs) with the phase-fronts parallel to the ionization layer surfaces are responsible for the tilt angles of sporadic plasma layers, we have developed a new technique for determining the parameters of IGWs linked with the inclined E_s structures. A small-scale internal wave may be modulating initially horizontal E_s layer in height and causing a direction of the plasma density gradient to be rotated and aligned with that of the wave propagation vector $\boldsymbol{k}$. The results of determination of the intrinsic wave frequency and period, vertical and horizontal wavelengths, intrinsic vertical and horizontal phase speeds, and other characteristics of IGWs under study are presented and discussed.

Keywords: Earth's ionosphere; Inclined plasma layer; Radio occultation; Internal gravity wave

1. Introduction

The radio occultation (RO) method is widely used in two-position remote sensing when a transmitter and receiver move from the opposite sides with respect to the planetary limb. Since 1964, this method has successfully been used for studying the stratified structure of planetary atmospheres and ionospheres (Kliore et al., 1965). With the advent of geostationary and navigation satellites, the RO experiments were started in order to study the three-dimensional structure of the Earth's ionosphere and atmosphere in the global scale (Ware et al., 1996). Use of high-stability and atomic-clock synchronized signals of navigational systems for studies of the Earth's atmosphere and ionosphere has significantly increased an efficiency of the RO method whose advantages are the high accuracy and spatial resolution, all-weather capability and long-term stability of global soundings, and a possibility of almost simultaneous measurements in the atmosphere and ionosphere (Kirchengast et al., 2004; Liou et al., 2010; Pavelyev et al., 2009a; Ware et al., 1996; Yakovlev et al., 2010). In terms of efficiency, the RO monitoring is

* Corresponding author at: Kotel'nikov Institute of Radio Engineering and Electronics of the RAS (Fryazino branch), Vvedensky square 1, 141190 Fryazino, Moscow Region, Russia.
E-mail address: vngubenko@gmail.com (V.N. Gubenko).

https://doi.org/10.1016/j.asr.2017.10.001
0273-1177/

comparable with global radio tomography used for remote sensing of the ionosphere by ground-based and satellite-borne means (Kunitsyn and Tereshchenko, 2003).

A spherical symmetry of the ionosphere and atmosphere, and coincidence of their symmetry centers are the main conditions underlying the radio occultation method. Once these conditions are fulfilled, the variations of the vertical gradient of refractive index in the ray perigee are the cause for the amplitude and phase variations of the RO signal recorded by a low-orbit satellite receiver (Igarashi et al., 2001). Intense frequency-dependent variations in the signal amplitude and phase which are often observed in the height interval 30–80 km of the ray perigee, located above the main part of the neutral atmosphere and below the ionospheric E layer, contradict an assumption of the global spherical symmetry (Sokolovskiy et al., 2002). This phenomenon can be explained by the influence of inclined plasma layers which are located in the ionosphere at usual altitudes of 90–130 km, but at significantly large distances from the ray perigee (Pavelyev et al., 2008, 2012, 2015; Wickert et al., 2004). A back-propagation method was proposed by Gorbunov et al. (2002) and Sokolovskiy et al. (2002) for determining the location of irregularities in the ionospheric E and F layers. Another method for measuring the plasma-layer inclination and displacement with respect to the ray perigee in the Earth's and Venusian ionospheres, which is based on the relationship between variations in the phase path acceleration and the intensity of the RO signal, was proposed in the works (Liou and Pavelyev, 2006; Pavelyev et al., 2009b, 2010).

Sporadic E (E_s) layers are known as the thin layers of enhanced ionization in the E region ionosphere at heights from 90 to 120 km. Knowledge of the E_s properties and effects is of great interest to radio communications and navigations. Wu et al. (2005) have studied global E_s morphology using CHAMP RO data. The E_s climatology was investigated with the SNR (signal-to-noise ratio) and phase variances in terms of monthly zonal means, seasonal maps, and diurnal and long-term variations (Wu et al., 2005). The very complete study on the global distribution of sporadic E-layer occurrence was made by Arras et al. (2008). In order to derive global information on small-scale ionospheric irregularities between January 2002 and December 2007, they used and analyzed a large data base of GPS RO measurements from CHAMP, GRACE and FORMOSAT-3/COSMIC. It was found that the global distribution of ionospheric irregularities shows strong variations with highest occurrence rates during summer in the middle latitudes. Similar results were also found to local level analyzing the occurrence of sporadic E_s over the Italian ionospheric stations (Pietrella and Bianchi, 2009; Pietrella et al., 2014). The maxima of E_s occurrence appear at the middle latitude zones between about 10° and 60° geomagnetic latitude. There are deep minima located at high latitudes where magnetic dip angles are larger than 70°–80° that agrees with the wind shear theory (Arras et al., 2008; Haldoupis, 2011).

The wind shear theory of the sporadic E-layer formation in middle latitudes has been confirmed by many investigations (Whitehead, 1989). The mid-latitude E_s layers have been shown to be very thin (as little as a few 100 m thick), widespread horizontally (several 100 s of km), dense (reaching densities as high as several times 10^6 electrons/ions per cm^3) and comprised of metallic atoms (Kirkwood and Nilsson, 2000). In the presence of inclined geomagnetic fields, the ion convergence in the E-region of the ionosphere can be caused by both zonal and meridional wind shears. However, the primary driver of ion convergence in the middle latitudes at altitudes below 115 km is considered to be zonal wind shear (Haldoupis, 2012). Associated with the convergence process of positive ions into a thin layer, electrons move along the geomagnetic field lines to neutralize the positive charge. It should be noticed that this wind shear theory explains the principle of layer formation in the vertical plane but not in the horizontal plane. In the daytime E-region, the molecules of N_2 and O_2 are the dominant molecules for ionization. However, their rapid recombination leads E-region ionization to photo-equilibrium, which is the reason why a normal E-layer almost disappears at night. On the other hand, sporadic E layers often occur at night and it is common that their appearances last for several hours. These facts contradict with the normal E-region photo-equilibrium and exclude it from the possible source of positive ions responsible for the E_s ionization. To confirm that metallic ions (Fe^+ and Mg^+) are the primary source of the E_s ionization, the electron and ion density profiles have been directly measured by the rocket observations (Roddy et al., 2004). As the theory predicts, recombination rates of these metallic ions are much lower than those of NO^+ and O_2^+. Metallic ions have long lifetimes: a few days at altitude of 120 km and a few hours at 95 km (Haldoupis, 2012). These metallic atoms are considered to be of meteoric origin and it is natural to consider that the formation of thin layers is attributed to the ion convergence by the neutral wind shears in the presence of geomagnetic field. Although, in some observations, meteor is observed to be trapped in the wind shear node to produce enhanced E_s layers, the primary mechanism is considered to be the existence of shears in the neutral winds (Maruyama et al., 2003, 2008; Malhotra et al., 2008).

In recent years, the structures of E_s layers and their horizontal shapes have been successfully imaged with ground-based radar observations during nighttime (Hysell et al., 2002, 2004; Larsen et al., 2007). Numerical simulations suggested that E_s patches are preferably aligned in the NW-SE direction and propagate southwestward in the Northern hemisphere (Cosgrove and Tsunoda, 2002, 2004; Yokoyama et al., 2009). However, it is necessary to have more observations of the E_s layers in the middle latitudes to substantiate such simulation results. Widely accepted structuring mechanisms of E_s under the presence of vertical wind shear include internal gravity waves (Woodman et al., 1991; Didebulidze and Lomidze, 2010;

Chu et al., 2011), or a neutral wind shear instability (Larsen, 2000; Bernhardt, 2002; Larsen et al., 2007; Hysell et al., 2009), or an E_s layer plasma instability forced by neutral wind shear (Cosgrove and Tsunoda, 2002, 2004). The atmospheric gravity waves are suggested to modulate E_s layer vertically which would cause quasi-periodic (QP) radar echoes. Tsunoda et al. (1994) have shown that the polarization electric field develops as the result of the altitude modulation in the nighttime, mid-latitude ionosphere and that its properties are similar to those of the atmospheric gravity waves. Deployment of coherent scatter radars in the modern ionospheric experiments made clear important structuring in the midlatitude ionization layers (Yamamoto et al., 1991, 1992). Rocket experiments have shown that QP echoes come from patchy sporadic E layers accompanied by strong polarization electric fields and neutral wind shears (Bernhardt et al., 2005; Yamamoto et al., 2005). Large wind shears were indeed seen in the two intensive rocket experiments combined with ground-based radar observations during the Sporadic-E Experiment over Kyushu (SEEK and SEEK-2) campaign (Larsen et al., 1998, 2005; Yokoyama et al., 2005). The shear or Kelvin-Helmholtz (K-H) instability in the neutral atmosphere is also proposed to create a densely ionized billow structure (Bernhardt, 2002). In fact, such billow structure in the E-region of the ionosphere is imaged as a trimethyl aluminum (TMA) trail in the up-leg portion of a rocket experiment conducted in the SEEK-2 campaign (Larsen et al., 2005). Observations of three-dimensional structures of descending and approaching echoes (Saito et al., 2006) can be explained by unstable regions that developed along the geomagnetic field line from E_s layer altitudes up to higher altitudes (>120 km). The interferometer measurement results obtained by Saito et al. (2006) support the model proposed in the works (Maruyama et al., 2000; Ogawa et al., 2002) and confirmed a computer simulation performed by Yokoyama et al. (2004).

At high latitudes (>60°), the wind shear mechanism would not be as efficient as at mid-latitudes due to the large inclination of the magnetic field which is almost vertical here. The large-scale horizontal structure of E-region plasma is therefore dominated by the spatial character of solar and particle precipitation sources. The two-stream and gradient drift instabilities are the primary plasma instabilities sources of structure in the auroral E region. Atmospheric gravity waves are somewhat less important as a source of vertical structuring at high latitudes due to the large dip angle of the magnetic field (Kelley, 2009). However, the small off-vertical angle is very important because of large-magnitude perpendicular electric fields. At high latitudes, convection electric fields often give the important driver for convergence or divergence in the ion motion (Nygren et al., 1984; Turunen et al., 1993; Bristow and Watkins, 1991, 1993; Kirkwood and von Zahn, 1991, 1993; Kirkwood and Nilsson, 2000). It was first suggested by Nygren et al. (1984) that sporadic E layers at high latitudes can be formed by the action of the electric field alone, since the wind shear mechanism is less effective, in particular below 110 km altitude. The electric field in the auroral zone and polar cap is appreciably larger and more widespread than in the equatorial region. The average auroral electric field has a strong diurnal component with an amplitude of 30 mV/m and maxima near 05:00 and 18:00 LT. Fields as high as 50 mV/m are common in both the oval and polar cap, and numerous measurements exceeding 100 mV/m have been reported (Kelley, 2009). Clear signatures of the influence that tidal winds (semidiurnal and diurnal modes) have on the formation of sporadic layers (disregarding electric fields) have also been observed (Pezzopane et al., 2016), but atmospheric gravity waves may provide additional wind nodes (Turunen et al., 1993). In fact, Lehmacher et al. (2015) have shown that, under very quiet conditions, a sporadic E layer can be produced mainly by the wind shear process, but even minimal electrical fields may be relevant at auroral latitudes. Cox and Plane (1998) have argued that E_s densities as high as 3×10^6 cm^{-3} are frequently seen at high latitudes and that, consequently, sufficient Na^+ is available to produce previously measured Na densities. The layer composition of metallic ions connects E_s to meteor ablation processes (Hunten et al., 1980) and the formation of neutral metal layers in the upper mesosphere (Kirkwood and von Zahn, 1991, 1993; Heinselman et al., 1998). In the polar cap, the mechanisms involving horizontal electric fields or neutral winds will not work because the vertical velocity is proportional to cosine of a magnetic dip angle that becomes 0.034 for the dip angle of 88° compared to 0.17 for the dip angle of 80° (Kelley, 2009). High-latitude or auroral E_s layers were assumed to be a manifestation of the aurora which corresponds to a strong sporadic source of enhanced ionization. But the ionization layers produced in this case are, actually, not particularly thin. According to Kirkwood and Nilsson (2000), there are several types of the high-latitude layers which are much thinner than those produced by auroral precipitation, and which are likely to be produced by processes similar to those producing sporadic E-layers at the middle latitudes. Watson et al. (2016) have presented statistical characteristics (occurrence rate, amplitude, and frequency) of low-frequency (<100 mHz) variations in total electron content (TEC) observed in the polar cap ionosphere by five GPS receivers over a 6 year period (2009–2014). Night-side occurrence of F and E region variations decreased with increasing latitude, which may be indicative of auroral activity expanding poleward from lower latitudes into the night-side polar cap. Increased substorm activity near solar maximum is associated with more frequent poleward expansion of auroral activity, and expansion of auroral activity deeper into the polar cap. Significant TEC variations due to high-energy particle precipitation (>10 keV electrons) in the night-side polar cap has previously been reported by Watson et al. (2011).

Based on the simulation and RO data analysis, Zeng and Sokolovskiy (2010) have found that the sporadic E_s

layer aligned with the wave propagation direction could cause defocusing of the radio waves, accompanied by the amplitude signal oscillations above and below the defocusing region due to interference of the direct and refracted RO rays. These effects result in specific U-shape patterns in the RO signal amplitude data, and this U shape will reduce and even disappear with the increase of the E_s tilt angle with respect to the wave propagation direction (Zeng and Sokolovskiy, 2010). An attempt to explain the sporadic E-layer formation on a base of comparing the FORMOSAT-3/COSMIC data with meteor and wind shear information was made by Yeh et al. (2014). Based on these comparison results, Yeh et al. (2014) have concluded that both the wind shear theory and meteor ionization mechanisms are essential factors in the E_s layer generation. The high-resolution GNSS (Global Navigation Satellite System) RO signals from multiple missions and collocated observations from lidar and ionosondes were used by Yue et al. (2015) for an investigation of the complex E_s layer structures. Yue et al. (2015) have shown an important case of the E_s occurrence in a broad region during a certain time interval, and obtained results have been validated by the independent collocated observations from ionosondes.

The goals of this paper are: (I) to present a method of deriving the location and tilt of plasma layers from RO data; (II) to conduct the case study of inclined sporadic E (E_s) layers in the high-latitude ionosphere of the Earth observed by CHAMP (Challenging Minisatellite Payload); (III) to present a new technique for determining the parameters of IGWs responsible for the tilts of studied E_s layers. The remainder of the paper is organized as follows. A method of deriving the location and tilt of ionospheric layers from RO data is given in Section 2. The results of analysis of the CHAMP RO data in the ionosphere are presented in Section 3. A new technique for determining the parameters of internal waves responsible for the tilts of observed sporadic E layers is described in Section 4. The calculation of characteristics of IGWs under study and the discussions are also given in Section 4, followed by a Summary.

2. A method for deriving the location and tilt of plasma layers from the RO data

A diagram of the RO experiments is shown in Fig. 1. The high-stability radio signals radiated by satellite G pass through the ionosphere and atmosphere along the GTL ray and are recorded by a receiver on board of another satellite L. The amplitude $A(t)$ and variations in the phase-path increase (eikonal) $\Phi(t)$ at the carrier frequency are recorded as functions of time t on board of satellite L. A global spherical symmetry of the ionosphere and atmosphere with the common center (point O in Fig. 1) is the key assumption when analyzing the experimental RO data. A small region with center at the tangential point T, where the radio ray is normal to the refractive index gradient, makes the main contribution to variations in amplitude and phase of the RO signal recorded by receiver L despite a significantly greater path length along the ray trajectory GTL (Igarashi et al., 2001). The length of this region on the ray trajectory GTL is equal to the horizontal resolution $\Delta_h = 2\ (2l_f\ r_e)^{1/2}$ in the RO method, where $l_f = (\lambda d_2)^{1/2}$ is the Fresnel-zone size, λ is the signal wavelength, r_e is the TO-segment length, and d_2 is the TL-segment length, that is approximately equal to the DL-segment length (Fig. 1). The quantity of Δ_h corresponds to the minimum horizontal layer length which is measured by the RO method. Contribution of this small region to the amplitude and phase variations under the standard ionospheric conditions is much greater than that from the remaining part of the GTL path (Igarashi et al., 2001). The tangential point, at which the GTL radio ray is normal to the refractive index gradient, coincides with the perigee T of the GTL ray trajectory under conditions of global spherical symmetry. The RO method allows us to determine the refractive coefficient and its vertical gradient along the trajectory of the GTL ray perigee with the high vertical resolution and accuracy.

An important relationship between the eikonal acceleration a and refractive attenuation $X_p(t)$ of the RO signal was obtained in the work (Liou and Pavelyev, 2006) and it has the form:

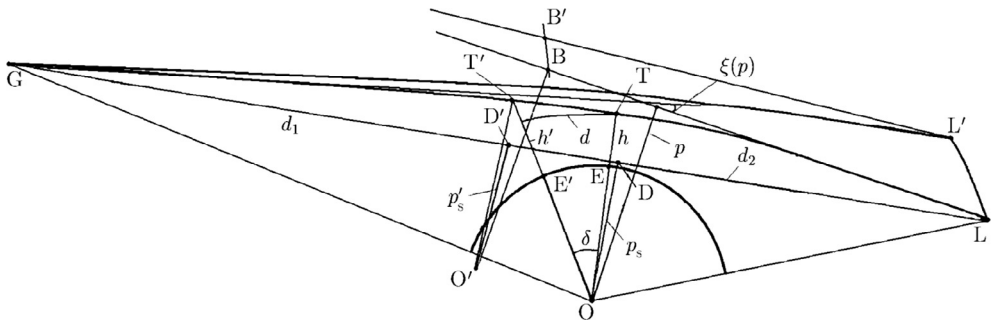

Fig. 1. Geometry of ray path in the radio occultation experiments.

$$1 - X_{\mathrm{p}}(t) = ma, \quad a = \mathrm{d}^2\Phi(t)/dt^2,$$
$$m = d_1 d_2/(R_0 \mathrm{d}p_{\mathrm{s}}/\mathrm{d}t)^2, \quad d_1 = R_0 - d_2, \tag{1}$$

where d_1, d_2, and R_0 are the distances along the straight lines GD, DL, and GL, respectively, while p and p_{s} are the impact parameters which correspond to the ray trajectory GTL and the line of sight GL. The value of m is taken from the satellite-borne observations. The distance d_2 is approximately equal to the length of the arc TL since the refractive angle $\xi(p)$ (Fig. 1) is small. Authors of the work (Liou et al., 2007) have shown that Eq. (1) is valid under the following condition:

$$\left|(p - p_{\mathrm{s}})\frac{\mathrm{d}R_{1,2}}{\mathrm{d}t}\right| \ll \left|p_{\mathrm{s}}\frac{\mathrm{d}p_{\mathrm{s}}}{\mathrm{d}t}\right|, \tag{2}$$

where R_1 and R_2 are the distances OG and OL, respectively. Inequality (2) is fulfilled during the RO sensing of atmospheres and ionospheres of the Earth and planets, since the absolute value of the difference $(p - p_{\mathrm{s}})$ is almost always much smaller than the impact parameters p and p_{s}.

Let us formulate a criterion for the coincidence of the tangential point with ray perigee. To this end, it is necessary and sufficient to require the global spherical symmetry of the atmosphere and ionosphere, and the absence of the multi-path propagation and random irregularities. Once these requirements are met and absorption is absent, Eq. (1) is valid and results in identical equality of refractive attenuations which are determined from the amplitude and phase variations of the radio occultation signal:

$$X_{\mathrm{p}}(t) \equiv X_{\mathrm{a}}(t), \quad X_{\mathrm{a}}(t) = I/I_0, \tag{3}$$

where I_0 and I are the RO signal intensities measured before and after the radio-ray entrance to the ionosphere, respectively. The integral absorption Γ in the atmosphere and/or ionosphere can be determined by excluding the refractive attenuation $X_{\mathrm{p}}(t)$, which was found from the eikonal measurements at one frequency, with the help of Eq. (1) and the relationship $\Gamma = 1 - X_{\mathrm{a}}(t)/X_{\mathrm{p}}(t)$ (Pavelyev et al., 2009b).

Identity (3) is the mathematical condition for finding the tangential point of the atmospheric or ionospheric layer in the ray perigee T. It is convenient to represent variations in the refractive attenuations, which are determined from the measured variations in the eikonal and amplitude variations of the RO signal at one frequency, in the form of analytic functions having the amplitudes $A_{\mathrm{p}}(t)$ and $A_{\mathrm{a}}(t)$ and the phases $\chi_{\mathrm{p}}(t)$ and $\chi_{\mathrm{a}}(t)$:

$$1 - X_{\mathrm{p}}(t) = ma = A_{\mathrm{p}}(t)Re\exp[j\chi_{\mathrm{p}}(t)],$$
$$1 - X_{\mathrm{a}}(t) = ma = A_{\mathrm{a}}(t)Re\exp[j\chi_{\mathrm{a}}(t)]. \tag{4}$$

The functions $A_{\mathrm{p}}(t)$ and $A_{\mathrm{a}}(t)$, and the functions $\chi_{\mathrm{p}}(t)$ and $\chi_{\mathrm{a}}(t)$ can be found from the known time dependence $1 - X_{\mathrm{p}}(t)$ and $1 - X_{\mathrm{a}}(t)$, e.g. using the numerical Hilbert transform or other methods of numerical data processing.

If absorption is absent, then under the condition of synchronous variations in the functions $1 - X_{\mathrm{p}}(t)$ and $1 - X_{\mathrm{a}}(t)$, we can obtain with allowance for Eq. (1) that:

$$A_{\mathrm{p}}(t) = A_{\mathrm{a}}(t), \quad \chi_{\mathrm{p}}(t) = \chi_{\mathrm{a}}(t). \tag{5}$$

When the condition of the global spherical symmetry is fulfilled, then Eq. (5) represents another form of the above-mentioned criterion.

Deviations from this criterion can be related to the multi-path propagation, diffraction, scattering, and the influence of turbulence and other atmospheric and ionospheric irregularities. In some cases, these deviations can be caused by the influence of horizontal gradients and the appearance of other tangential points in the ionospheric parts of a radio ray, e.g. the tangential point T′ (Fig. 1). This leads to a displacement of the spherical-symmetry center from the point O to point O′ (Fig. 1), and Eq. (2) takes the form:

$$\left|(p' - p'_{\mathrm{s}})\frac{\mathrm{d}R'_{1,2}}{\mathrm{d}t}\right| \ll \left|p'_{\mathrm{s}}\frac{\mathrm{d}p'_{\mathrm{s}}}{\mathrm{d}t}\right|, \tag{6}$$

where R'_1 and R'_2 are the distances O′G and O′L, respectively.

Eq. (6) is also valid in almost all important cases. Here, the tangential point T′ coincides with the new perigee of a radio ray with respect to the center O′, and the criterion from Eq. (3) is fulfilled in the form:

$$X'_{\mathrm{p}}(t) \equiv X_{\mathrm{a}}(t), \tag{7}$$

where $X'_p(t)$ is the refractive attenuation calculated from:

$$1 - X'_{\mathrm{p}}(t) = m'a, \quad a = \mathrm{d}^2\Phi(t)/\mathrm{d}t^2,$$
$$m' = d'_1 d'_2/(R_0 \mathrm{d}p'_{\mathrm{s}}/\mathrm{d}t)^2, \quad d'_1 = R_0 - d'_2, \tag{8}$$

where m' stands for the parameter m which corresponds to the spherical-symmetry center O′ (Fig. 1), d'_2 is the distance D′L, and p'_s is the impact parameter that corresponds to the line of sight GL and the center O′. The first Eq. (8) differs from Eq. (1) by new values of the refractive attenuation $X'_p(t)$ and the factor m' for the same value of the eikonal acceleration a.

Eqs. (7) and (8) allow us to determine the distance d between the ray perigee T and the new tangential point T′ in the absence of absorption. According to Eqs. (1), (7), and (8), as well as the condition (6), Eq. (5) should be fulfilled:

$$A'_{\mathrm{p}}(t) = A_{\mathrm{a}}(t), \quad \chi'_{\mathrm{p}}(t) = \chi_{\mathrm{a}}(t), \tag{9}$$

where $A'_p(t)$ and $\chi'_p(t)$ are the amplitude and phase of variations in an analytic representation of the refractive attenuation $1 - X'_p(t)$. By virtue of Eq. (3), the refractive attenuation obtained from amplitude experimental data is independent of the spherical-symmetry center location. It follows from Eqs. (8) and (9) that the function $A'_p(t)$ is related to the amplitudes $A_{\mathrm{p}}(t)$ and $A_{\mathrm{a}}(t)$ by:

$$A'_{\mathrm{p}}(t) = \frac{m'}{m} A_{\mathrm{p}}(t) = A_{\mathrm{a}}(t), \quad A_{\mathrm{p}}(t) = \frac{m}{m'} A_{\mathrm{a}}(t). \tag{10}$$

If a displacement of spherical-symmetry center satisfies the conditions:

$$d_2/R_0 \ll 1, d'_2/R_0 \ll 1, \mathrm{d}p_{\mathrm{s}}/\mathrm{d}t \approx \mathrm{d}p'_{\mathrm{s}}/\mathrm{d}t, \tag{11}$$

then the last relationship in Eq. (10) can be written in the form:

$$A_{\mathrm{a}}(t) = \frac{d'_2}{d_2} A_{\mathrm{p}}(t). \tag{12}$$

From Eq. (12), one can find the following relationship for a displacement d of the tangential point T′ with respect to the ray perigee T:

$$d = d'_2 - d_2 = d_2 \frac{A_{\mathrm{a}} - A_{\mathrm{p}}}{A_{\mathrm{p}}}, \quad d_2 = \sqrt{R_2^2 - p_{\mathrm{s}}^2}. \tag{13}$$

Eq. (13) establishes the following rule: a displacement of the tangential (turning) point of the ray trajectory is determined by the relationship between the amplitudes A_{a} and A_{p}, which are obtained from variations in the intensity and eikonal of the RO signal. A displacement d is positive (negative) depending on the sign of a difference $(A_{\mathrm{a}} - A_{\mathrm{p}})$, while the tangential point T′ in this case is located in a part of the ray trajectories GT or TL, respectively. In this case, the phases $\chi_{\mathrm{p}}(t)$ and $\chi_{\mathrm{a}}(t)$ should be identical within the accuracy determined by the measurement error.

Eq. (13) holds when one of the satellites is located at a much greater distance from the perigee point T than the other satellite. This condition is fulfilled when the spacecraft–Earth communication lines are used in the RO experiments, or when the low-orbit satellites working with radio signals of the space navigation systems are used. If the displacement d is known, we can determine the height correction Δh to the actual layer height (h') and its angle δ of inclination with respect to the local horizon (Wickert et al., 2004):

$$\delta = d/r_{\mathrm{e}}, \quad \Delta h = d\delta/2 = d^2/(2r_{\mathrm{e}}), \quad h' = h + \Delta h, \tag{14}$$

where a parameter r_{e} is equal to the distance TO and h is the ray perigee height (Fig. 1).

This method can be compared with the back-propagation method for determining the location of ionospheric plasma irregularities, which was introduced by Gorbunov et al. (2002) and Sokolovskiy et al. (2002). According to the results of indicated works, in order to determine the radio fields between a transmitter and receiver, the electromagnetic field measured along the orbital trajectory LL′ is integrated with the Green's function corresponding to the spherical-wave field in free space. In this case, according to the back-propagation method, the field is determined along the straight lines which are tangent to the RO ray at any point in the line LL′ (Gorbunov et al., 2002). Using the back-propagation method, we find the region in which the amplitude modulation of an electromagnetic field is absent or minimum. The coordinates of this region determine the irregularity location. According to Vorob'ev et al. (1997), this region is located along the phase screen (line BB′ in Fig. 1), where the rays corresponding to the back-propagation field are normal to the directions laid off from the spherical-symmetry center O′ (straight lines O′B and O′B′ in Fig. 1). The curve BB′ is close to the straight line since the refractive angle is small. Inaccuracy in determining the length of the segment T′L by the back-propagation method is equal to the distance between the curve BB′ and the point T′: $\mathrm{T'B} \approx p'\xi/2$ (Fig. 1). The proposed method is used for determining the layer displacement d with respect to the radio-ray perigee. Therefore, the systematic error of the introduced method is smaller than that of the back-propagation method.

3. Analysis of the satellite CHAMP/GPS RO data in the ionosphere

To demonstrate a possibility of determining the location and inclination of ionospheric layers, we make an analysis of the CHAMP RO data, which were obtained using the radio signals at the GPS (Global Positioning System) frequency of 1575.42 MHz (the session of July 28, 2003 starting at 21:08 LT with the ray perigee coordinates 71.4°N and 67.3°W). The profiles of the CHAMP RO phase and amplitude data have the time resolution of 0.02 s, corresponding to the sample rate of 50 Hz. These data indicate the presence of intense quasi-regular amplitude and phase variations of the radio occultation signal. The refractive attenuations X_{a} and X_{p} of the RO signals obtained by processing the intensity and eikonal variations are shown in Fig. 2-I (curves 1 and 2) as functions of the perigee height h of ray trajectory GTL. The eikonal acceleration a was determined numerically by the twofold differentiation of the second-degree polynomial which was developed by the method of least squares in the sliding time interval $\Delta t = 0.5$ s. With a vertical ray speed of about 2.1 km/s, the height interval of ray penetration to the ionosphere for this time is of 1 km, and it corresponds to the vertical size of the Fresnel zone. The refractive attenuation X_{p} was obtained from Eq. (1) using the values of parameter a found from experimental data. The quantity m was taken from the satellite data. The refractive attenuation X_{a} was determined on the base of amplitude data using the method of least squares with averaging over the same time interval 0.5 s.

Variations in the refractive attenuations X_{a} and X_{p} are coherent, and that is indicative on the equality of phases χ_{a} and χ_{p}. Variations in the attenuations X_{a} and X_{p} are apparently caused by the influence of ionospheric layers in three intervals of the ray perigee height h of the ray trajectory GTL, which are denoted by a, b, and c in Fig. 2-I. The intervals a, b, and c correspond to the ray perigee height h in the ranges 50–72 km, 72–92 km, and 92–116 km, respectively. The signals $(X_{\mathrm{a}} - 1)$ and $(X_{\mathrm{p}} - 1)$ are coherent in the above-mentioned intervals. However, the

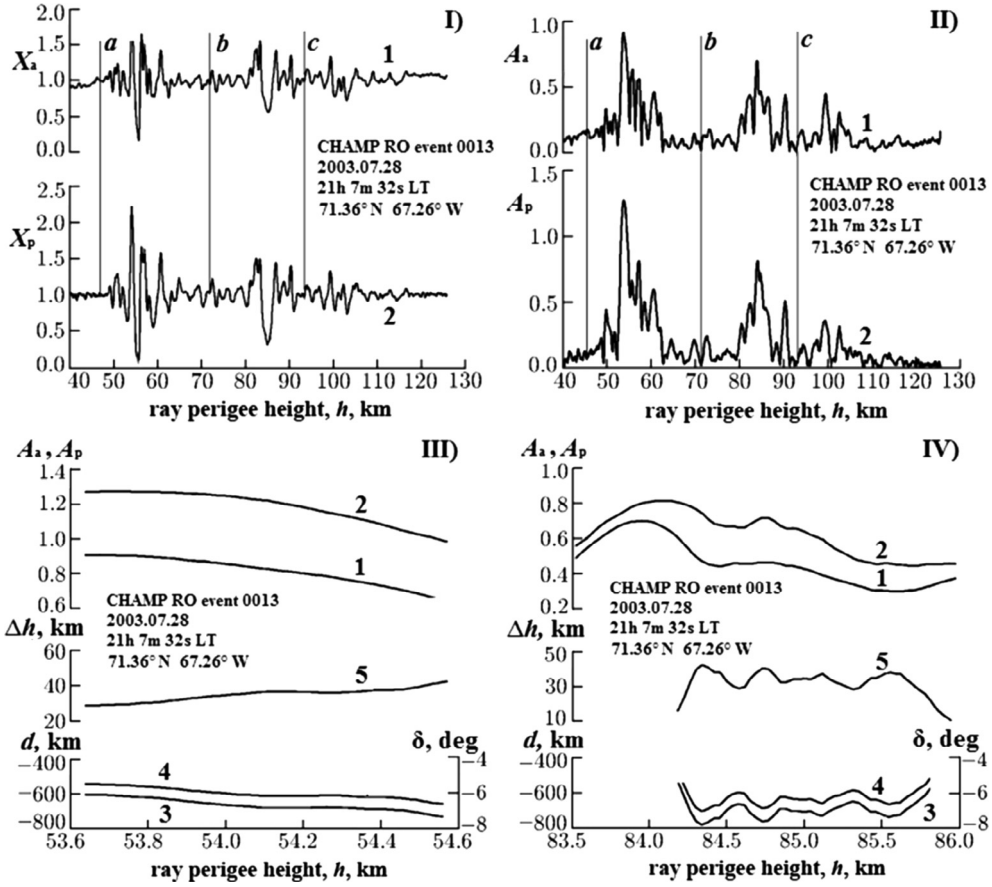

Fig. 2. Comparison of the refractive attenuations X_a and X_p obtained from the intensity and eikonal variations of the CHAMP RO signal at GPS frequency $f_1 = 1575.42$ MHz (curves 1 and 2 in panel I, respectively). Amplitudes A_a and A_p of analytical signals related to the variations of the refractive attenuations X_a and X_p (curves 1 and 2 in panel II, respectively). Determination of the location and slope for the first layer using amplitudes A_a and A_p (panel III). Determination of the location and slope for the second layer using amplitudes A_a and A_p (panel IV).

amplitudes A_a and A_p of analytic functions $(X_a - 1)$ and $(X_p - 1)$ in these intervals are different. The amplitudes A_a and A_p, which are determined with the help of numerical Hilbert transform, are shown in Fig. 2-II (curves 1 and 2, respectively). The amplitude values of A_a in the intervals a and b are smaller than the corresponding A_p values (Fig. 2-II). The opposite case is observed in the interval c (Fig. 2-I and -II). The first two layers from intervals a and b correspond to the negative values of displacement d. These two layers are located on the ray trajectory GTL between the points T and L. The upper layer from the interval c is displaced from the ray perigee T towards the navigation satellite G (Fig. 1). In the case of a non-zero layer displacement d, the values of actual layer height h' and ray perigee height h will not equal to each other, and they will differ by quantity Δh determined from Eq. (14). It is important to note that the height position of a layer is not uniquely determined by the ray perigee height h value. For example, two layers with the same value of perigee height h and different magnitudes of displacement d, according to Eq. (14), will have different values of actual layer height h'. Therefore, an actual layer height h' is appropriate and sufficient parameter for description of altitude position of a layer.

Some investigations have shown that not only a single sporadic E-layer, but much more complicated sporadic structures (double-peaks E_s, and even a rectangular E_s layer) can be observed (Yue et al., 2015). Complex profiles of sporadic E-layers may be caused by unstable wind shears. Bernhardt (2002) pointed out the drivers responsible for the plasma instability (e.g., the Kelvin-Helmholtz instability) could deform the E_s layer into a complex structure. These drivers could lift up part of the E_s layer to overlap with the original layer (Yue et al., 2015). As it is seen from Fig. 2-I, the layer a has complex (double) quasi-periodic structure. It is possible that the observed vertical undulation shows indications of propagating an internal gravity wave through the layer. The first (lower) part of this layer located at a ray perigee height of 55 km has a vertical size of 3.0 km, and its second (upper) part located at a perigee height of 59 km has a vertical size of 4.4 km. The layer b located at a ray perigee height of 85 km has a vertical size of 4.4 km also, and it has typical U-shape structure, as reported by Zeng and Sokolovskiy (2010), with oscillations

above and below of the defocusing region due to the interference of direct and refracted radio rays. The layer *c* located at a perigee height of 103 km has a vertical size of 3.0 km. As it is seen from Fig. 2-I, this layer is less pronounced than underlying layers *a* and *b*.

The developed method can be used for determining the ionospheric layer location on the ray trajectory GTL, since variations in the refractive attenuations X_a and X_p are coherent. The results of determining the layer displacement *d* in intervals *a* and *b* are shown in Fig. 2-III and -IV. Curves 1, 2, and 3 in Fig. 2-III and -IV correspond to the perigee height dependence of amplitudes A_a and A_p, and displacement *d*, respectively. Curves 4 in Fig. 2-III and -IV indicate the layer inclination angle δ that is shown in degrees (right vertical scales). Curves 5 represent the correction values Δ*h* [km] to the actual layer height *h*′ for the layer *a* (Fig. 2-III) and layer *b* (Fig. 2-IV), respectively. Variations in the displacement *d* are concentrated in the ranges from −630 to −800 km and from −600 to −750 km (intervals *a* and *b*, respectively, interval *c* isn't shown). The statistical error of estimating the ratio $(A_a - A_p)/A_p$, using Eq. (13), is minimal when the A_p value is maximal. If the relative error in the measurement of A_p is 5%, then the accuracy of estimating *d* is about ±100 km. On average, the values of displacement in the intervals *a* and *b* are equal to $d = -730$ km and $d = -620$ km, correspondingly. The estimated mean value of the displacement *d* in the interval *c* is positive and equal to $d = 620$ km. According to Eq. (14), one can find that the inclination angles of plasma layers *a*, *b*, and *c* with respect to the local horizontal direction are approximately equal to $\delta = -7.3° \pm 0.9°$, $\delta = -6.4° \pm 0.9°$, and $\delta = 6.4° \pm 0.9°$, respectively. The correction magnitudes Δ*h* to the actual layer height *h*′ for the layer *a* (Δ*h* = 40 km), layer *b* (Δ*h* = 30 km) and layer *c* (Δ*h* = 30 km) have been also determined. On the base of the obtained mean values of layer displacement in the intervals *a*, *b*, *c*, and geometry of the real RO experiment under study, we have found the corrected layer coordinates: 64.0°N, 66.5°W (layer *a*); 65.0°N, 66.9°W (layer *b*); 77.5°N, 69.0°W (layer *c*). Using indicated corrected coordinates for layers *a* and *b*, we have found that the time by 1 h 35 m UT on 29 July 2003 corresponds to the measurement time of 21 h 7 m 32 s LT for the our case study. The CHAMP RO event 0013 was observed in the nighttime high-latitude or auroral E_s region during a moderate geomagnetic activity. The value of the three-hourly magnetic activity index K_p in the interval 1–3 h UT on 29 July 2003 was $K_p = 4-$ (http://wdc.kugi.kyoto-u.ac.jp/cgi-bin/kp-cgi). The value of the hourly magnetic deflection index D_{st} at 2 h UT on 29 July 2003 was only of −3 nT (http://wdc.kugi.kyoto-u.ac.jp/dst_final/200307/index.html). It should be noted that the time period of CHAMP RO measurements was preceded by an intense storm activity from 18 h UT on 26 July to 10 h UT on 28 July 2003 (http://www.izmiran.ru/ionosphere/weather/storm/tecstorm.txt). The peak of a storm activity was by 2 h UT on 27 July with the value of the W_p-max index about 6.3 (intense storms are included with threshold: W_p-max > 5.0). The highest value of the K_p index during the intense storm ($K_p = 6$) was encountered only once. This took place in the interval 18–20 h UT on 26 July 2003 (http://wdc.kugi.kyoto-u.ac.jp/cgi-bin/kp-cgi).

The local spherical symmetry allows us to apply the Abel transform for solving the inverse problem and finding the distributions of electron density and its gradient in the layer (Pavelyev et al., 2009b). The resulting dependence of the electron density $N_e(h')$ and its gradient dN_e/dh' are shown in Figs. 3 and 4, correspondingly. Height profiles of the electron density N_e and vertical gradient dN_e/dh' for the layers *a*, *b* and *c* were retrieved from the RO eikonal data. The corrected actual layer height *h*′ and ray perigee height *h* for the layers are shown on the top and bottom horizontal axes in Figs. 3 and 4. The electron density maxima heights for layers *a*, *b* and *c* are indicated by arrows in Fig. 3. It is important to note that the electron density maxima heights coincide with the refractive attenuation minima heights for layers *a*, *b* and *c*. This fact fully corresponds to the results obtained by Zeng and Sokolovskiy (2010), and it may be easy seen from comparison of Figs. 2-I and 3. When the single sporadic E-layer is aligned with the propagation direction, its central part (electron density peak) results in the defocusing of radio waves, while the edge parts results in the focusing (Zeng and Sokolovskiy, 2010). The layers *a* and *b* are located on the ray part LT at approximate distances of 730 and 620 km from point T, respectively, with maximum gradients at the actual layer heights of 95 and 114.5 km, correspondingly (Fig. 4A and B). The layer *c* is located in the ray part GT at a distance of about 620 km from point T with the vertical gradient maximum at an actual layer height of 130 km. According to Fig. 4, the vertical gradient variations of electron density in the layers *a*, *b*, and *c* are concentrated in the intervals:

$$-3.0 \cdot 10^5 \text{ cm}^{-3}/\text{km} < dN_e(h')/dh' < 5.6 \cdot 10^5 \text{ cm}^{-3}/\text{km},$$
$$-2.4 \cdot 10^5 \text{ cm}^{-3}/\text{km} < dN_e(h')/dh' < 8.5 \cdot 10^5 \text{ cm}^{-3}/\text{km},$$
$$-1.7 \cdot 10^5 \text{ cm}^{-3}/\text{km} < dN_e(h')/dh' < 2.8 \cdot 10^5 \text{ cm}^{-3}/\text{km}.$$

These values of variations are typical for the intense sporadic E-layers in the Earth's ionosphere observed from ground-based remote sensing, in situ techniques, and satellite sensors (Kelley, 2009; Mathews, 1998; Whitehead, 1989). The height interval of amplitude variations is approximately equal to the height interval of variations in the electron density and its gradient.

4. Coupling between the tilted plasma layers and internal waves

Wave processes have a significant effect on the circulation, chemical composition, thermal conditions, and variability of planetary atmospheres. In the first place, an important role of the internal gravity waves (IGWs) is due to the fact that they provide the effective mechanism of energy and momentum transfer from the lower

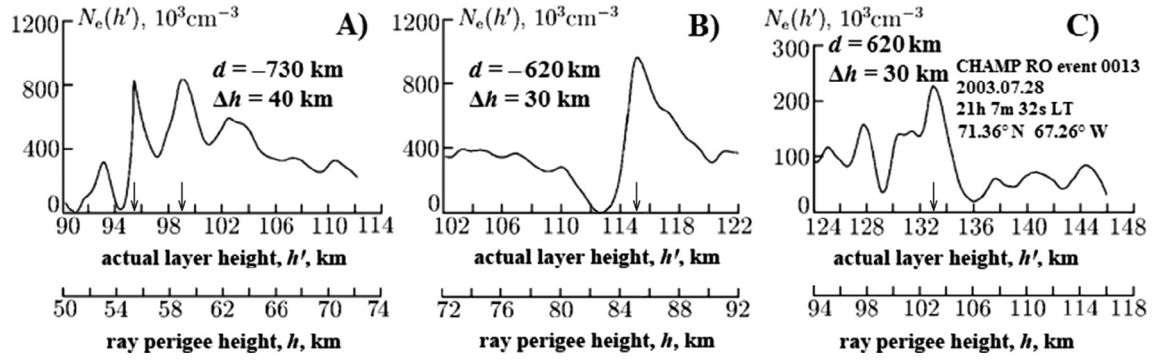

Fig. 3. Results of determining the electron density for three ionospheric layers. A displacement and height correction of plasma layers are: $d = -730$ km and $\Delta h = 40$ km (layer a, panel A); $d = -620$ km and $\Delta h = 30$ km (layer b, panel B); $d = 620$ km and $\Delta h = 30$ km (layer c, panel C). The electron density maxima heights for layers a, b and c are indicated by arrows.

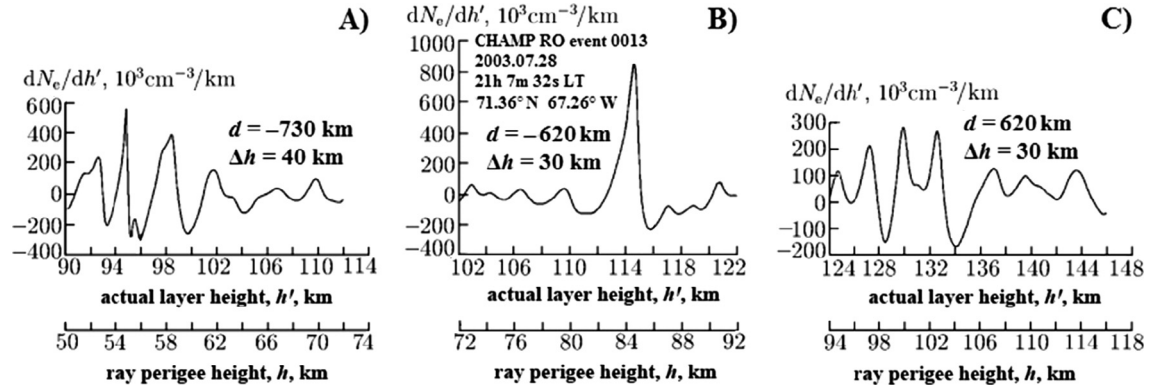

Fig. 4. Results of determining the vertical gradient for three ionospheric layers. A displacement and height correction of plasma layers are: $d = -730$ km and $\Delta h = 40$ km (layer a, panel A); $d = -620$ km and $\Delta h = 30$ km (layer b, panel B); $d = 620$ km and $\Delta h = 30$ km (layer c, panel C).

atmospheric levels to the top. Sources generating the internal waves in an atmosphere may be the thermal contrasts near the surface, topography, shear wind instability, convection, and frontal processes. In the Earth's atmosphere, in the absence of energy dissipation, an amplitude of the wave disturbances of wind velocity or temperature increases approximately exponentially with increasing altitude, and therefore, the disturbances with small amplitude near the surface can produce significant effects at high altitudes, where the wave breaking and the transfer of wave energy and momentum in the undisturbed flux occur.

Probing the IGWs by any methods faces challenges, the essence of which is that the parameters measured are parameters of a disturbed atmospheric state, for example, wind velocity, temperature, or density, and from this measurement it is necessary to determine which part of the "signal" is caused by IGWs. Here, the general approach is to separate the small-scale variations from the slow background variations, and assume that these small-scale variations are associated with the internal wave phenomena. Approaches using any scale separation should take into account that not all small-scale variations in the atmosphere are caused by IGWs, and not all internal waves have small scales. Analyzed variations can be connected not only with the internal wave influence, but also with that of the regular thin layers or turbulence in an atmosphere (Gubenko and Andreev, 2003, 2007; Gubenko et al., 2008a; Yakovlev et al., 1991). For the correct interpretation of measurement results, it is necessary to have physically reasonable criteria for the identification of each factor potentially affecting measurement results. An advantage of the radio occultation measurements for studying the internal waves in an atmosphere is the wide geographical and temporal coverage of studied areas, allowing one to perform the global monitoring of wave activity in a planetary atmosphere. It has been believed until the present time that on the base of the RO measurements alone it is impossible to estimate such key wave parameters as the intrinsic frequency, or the horizontal and vertical phase velocities which are needed to quantify the internal wave effects.

Gubenko et al. (2008b, 2011, 2012, 2015) have developed an original method that can be used to identify the discrete (narrow spectral) wave events, and to determine the parameters of identified IGWs from a data analysis of the individual vertical profile of temperature, or density, or Brunt-Vaisala frequency squared in a planetary atmosphere. At the same time, this new method does not require any additional information not contained in the analyzed profile. An application of the developed technique to the

satellite RO data analysis makes it possible to study the wave activity at a global scale in the Earth's and Martian atmospheres, and to find the key internal wave parameters such as the intrinsic frequency, horizontal and vertical wavelengths, amplitudes of horizontal and vertical disturbances of wind velocity, the kinetic and potential and total wave energy per unit mass, vertical fluxes of wave energy and horizontal momentum (Gubenko et al., 2011, 2015, 2016a, b).

Internal gravity waves at the ionospheric heights can produce irregularities in ionization (Hines, 1960). For instance, the traveling ionospheric disturbances (TIDs) and some types of sporadic E irregularities are now known to be generated by these atmospheric IGWs. It has been found that the TIDs are characterized by a pronounced slope of the equal phase surfaces, while the almost horizontal surfaces of equal phases are detected in the sporadic E layers. This is mainly due to the fact that the latter are formed by components of atmospheric tides and long-period buoyancy waves, which are destroyed by dissipative effects in the ionospheric F region (Gossard and Hooke, 1975). It has been found by Whitehead (1972) that the amplitude of IGWs is about the same or greater than the amplitude of tidal waves in the E region. According to Hines (1960), the inclined fronts of TIDs should represent the phase fronts of buoyancy waves associated with the TIDs, and the downward phase propagation is due to the upward propagation of wave energy. It is necessary to note that more recent works (e.g. Otsuka et al., 2009) have suggested that medium-scale TIDs (MSTIDs) are associated with polarized electric field perturbations. This is because the most of nighttime MSTIDs propagate southwestward, and the preferred propagation direction cannot be explained by classical theory of internal gravity waves. An ionospheric instability that acts through electrodynamical processes involving polarized electric fields could develop the MSTIDs (Otsuka et al., 2009). Linkage of the sporadic E layers to other ionospheric phenomena, including spread F and TIDs has been also investigated (Tsunoda and Cosgrove, 2001).

When an internal gravity wave propagates through the ionosphere it sweeps the ionization into a wave-like distribution by collisions between the charged and neutral particles. Kato et al. (1970) have demonstrated that a gravity wave propagating through the E region produces a wave-like variation in the electron density which has the same frequency and wave numbers as the original IGW provided there are no boundaries or non-uniformities in the ambient plasma. Chimonas and Axford (1968) have found that the wind shear will tend to converge the ionization to the IGW node which moves downwards, and this dumping of the ionization from higher to lower heights is known as the corkscrew effect. Chimonas (1971) has considered the role of small-scale IGWs in producing horizontal convergence within a plasma layer formed in the basic tidal system. He has indicated that in the case of an IGW with downward vertical phase speed somewhat larger than the descent speed of the plasma layer, the layer ions "see" an almost stationary IGW wind-structure that sweeps ions through horizontal convergence/divergence zones producing the characteristic "patchiness" of the sporadic E layer. Forced spatial resonance occurs when an ionization irregularity formed by some other means (e.g. wind shears due to the atmospheric tides and/or long-period inertial gravity waves) has a drift velocity that coincides with the phase velocity of an internal wave and is also positioned so that the layer coincides with the peaks of the ionization irregularities produced by the atmospheric wave (Whitehead, 1971).

The internal gravity wave signatures are clearly seen for many high-latitude E_s observations, including a very nice example for Sondrestrom (67.0°N, 51.0°W, dip angle is 80°) near Kangerlussuaq, Greenland (Heinselman et al., 1998). The measurements were collected on the night of 10–11 December 1997 in the period of auroral activity at Sondrestrom. Sporadic E layers were observed to appear at an altitude of 105 km and then descend, settling in near 93 km altitude. Sodium lidar measurements from the same time period and altitude region have shown a well-formed background sodium layer extending from around 80 to 100 km throughout the measurement period. Around 2:00 UT, a 1 km-thick sporadic sodium layer began to form at 93 km altitude. The layer remained for at least 3 h, finally dissipating some time after 5:00 UT. There is an indication of the upward propagating internal gravity wave (downward-moving phase front) through the E_s layer with a ground-based wave period of 30 min (Heinselman et al., 1998). MacDougall et al. (2000a,b) observed similar E_s undulations at Eureka and Resolute Bay on January 1, 1995. They have shown the E_s structures which can be seen to be an intermingling of discrete U-shaped features. There appears to be a periodicity of about 30 min in some of the features, especially for the Eureka data. Note that Eureka also seems to sometimes have multiple height features (see the two E_s features at 07:00 and 07:30 UT, Fig. 6 of MacDougall et al., 2000a), and the lower height feature is delayed relative to the upper feature. These features are strong evidence for the action of gravity waves which are an important component of the formation mechanism of these E_s layers. Interpretation by MacDougall et al. (2000a,b) of these measurements is that the E_s bands are caused by gravity waves, and the band speed is the gravity wave speed. These particular gravity waves have been "selected" because they approximately satisfy the condition for spatial resonance (i.e. their phase velocity approximately matches the convection velocity). In their explanation, MacDougall et al. (2000a,b) have assumed that spatially resonant gravity waves are associated with the height-spread E_s layer. Turunen et al. (1993) have observed a set of steeply descending "intermediate layers", merging to the lower lying sporadic E layer. Descending "intermediate layers" differ from the main sporadic layers by their rapid downward motion and repetition period of about an hour. Both of these properties strongly suggest that

these high-latitude E_s layers are caused by internal gravity waves (Turunen et al., 1993).

Assuming an adiabatic inviscid process and small-scale motions, the perturbation equations for atmospheric motions can be derived from the fundamental equations for the atmospheric dynamics such as the equation of motion, first law of thermodynamics, continuity equation and equation of state for an ideal gas. If an internal gravity wave is a plane wave, we can derive the dispersion equation of a gravity wave, when $f^2 < \omega^2 < N_b^2$ and $m^2 >> 1/(4H^2)$, as follows (Fritts and Alexander, 2003; Gubenko et al., 2008b, 2012):

$$\frac{\omega^2 - f^2}{N_b^2 - \omega^2} = \frac{k_h^2}{m^2} = \frac{\lambda_z^2}{\lambda_h^2} = \tan^2\delta, \tag{15}$$

where H is the scale height in the atmosphere, N_b is the background Brunt-Vaisala frequency, f is the inertial frequency, and ω is the intrinsic frequency (frequency observed in the frame moving with the background flow) of an internal wave. The inertial frequency (Coriolis parameter) f is defined as $f = 2\Omega \sin\phi$, where $\Omega = 7.292\cdot10^{-5}$ rad/s is the Earth's rotation rate and ϕ is latitude. The intrinsic horizontal phase speed c_{ph}^{in} can be written as $c_{ph}^{in} = (c - \bar{u}) = \omega/k_h$, where c is the horizontal phase speed of an internal wave observed in the ground-based frame, and $\bar{u}$ is the component of mean horizontal wind speed in the direction of horizontal wave propagation vector $\boldsymbol{k_h}$. Parameters $k_h = 2\pi/\lambda_h$ and $m = 2\pi/\lambda_z$ represent the horizontal and vertical wave numbers, where λ_h and λ_z are horizontal and vertical wavelengths, respectively. An angle δ is that between the local vertical (axis z) and the wave propagation vector (k_h, m). According to the definition of intrinsic vertical phase speed c_{pz}^{in}, we have $c_{pz}^{in} = \omega/m$. The values of scale height H change from 5.3 to 11 km in the height interval 50–130 km under study (Gossard and Hooke, 1975). It is easy to show that in this height interval, an inequality $m^2 \gg 1/(4H^2)$ and Eq. (15) will be valid for internal waves with wavelengths $\lambda_z < 4H_{\min} \approx 21$ km. Taking into account an angle δ introduced earlier, the dispersion equation may be rewritten as:

$$\omega^2 = \frac{N_b^2 \tan^2\delta + f^2}{\tan^2\delta + 1}. \tag{16}$$

Our purpose in this Section is to study the internal wave modulation of existing E_s layers. For simplicity, let us assume that a horizontal E_s layer has formed because of wind shear before the interaction with IGWs begins. A small-scale internal wave may be modulating this, initially horizontal, E_s layer in height and causing a direction of the plasma density gradient to be rotated and aligned with that of the wave propagation vector $\boldsymbol{k}$. An idea of experimental determination of characteristics of an internal gravity wave associated with the inclined E_s structures is the following. We assume that an IGW propagating through the E region is responsible for the tilt of a sporadic horizontal plasma layer, and consequently the phase-front of an internal wave is parallel to the ionization layer surface. In this scenario, an angle δ between the local vertical and the wave propagation vector (see Eq. (16)) will be coincide with the inclination angle of a studied plasma E_s layer a, or b, or c (see results in Section 3). For determination of the wave parameters from Eq. (16), it is necessary to have the estimates of background Brunt-Vaisala frequency, N_b at the actual layer heights, h' where sporadic E layers a, b and c were really located. Because of the data about N_b at actual heights of the ionospheric E layer location are fairly conservative, then we used the reference atmosphere data given by Gossard and Hooke (1975): N_b ($h' = 95$ km) $\approx 2.3\cdot10^{-2}$ rad/s; N_b ($h' = 99$ km) $\approx 2.2\cdot10^{-2}$ rad/s; N_b ($h' = 115$ km) $\approx 2.1\cdot10^{-2}$ rad/s. These N_b-values correspond to the buoyancy periods ($\tau_b = 2\pi/N_b$) from 4.6 to 5.0 min, and they match to the vertical structure of the buoyancy period τ_b, computed for a standard atmosphere, that is given by Kelley (2009) on page 276 (see Fig. 6.5). From data presented in Fig. 6.5 by Kelley (2009), it was determined that N_b ($h' = 133$ km) $\approx 2.3\cdot10^{-2}$ rad/s. Using these estimates and obtained experimental results, we have found after calculations that: $1 \gg \tan^2\delta$, and $\omega^2 \gg f^2$. Taking into account these inequalities, the dispersion equation and wave parameter expressions will have a very simple form:

$$\omega/N_b = \lambda_z/\lambda_h = |\tan\delta|, \tau_i = 2\pi/\omega, |c_{ph}^{in}| = \omega/|k_h| = N_b/|m|, |c_{pz}^{in}| = \omega/|m| = N_b|\tan\delta|/|m|, \tag{17}$$

where τ_i is the intrinsic period of an internal wave.

Finally, let us calculate, using Eq. (17), the characteristics of internal waves responsible for the tilts of sporadic E layers in the case study:

Layer (lower) a ($h' = 95$ km, $\Delta h = 40$ km): $\lambda_z = 3.0$ km; $\delta = -7.3°$; $|\tan\delta| = 0.13$; $\lambda_h = 23.1$ km; $|c_{ph}^{in}| = 11.0$ m/s; $|c_{pz}^{in}| = 1.4$ m/s; $N_b = 2.3\cdot10^{-2}$ rad/s; $\omega = 3.0\cdot10^{-3}$ rad/s; $\tau_i = 34.9$ min.
Layer (upper) a ($h' = 99$ km, $\Delta h = 40$ km): $\lambda_z = 4.4$ km; $\delta = -7.3°$; $|\tan\delta| = 0.13$; $\lambda_h = 33.8$ km; $|c_{ph}^{in}| = 15.4$ m/s; $|c_{pz}^{in}| = 2.0$ m/s; $N_b = 2.2\cdot10^{-2}$ rad/s; $\omega = 2.9\cdot10^{-3}$ rad/s; $\tau_i = 36.1$ min.
Layer b ($h' = 115$ km, $\Delta h = 30$ km): $\lambda_z = 4.4$ km; $\delta = -6.4°$; $|\tan\delta| = 0.11$; $\lambda_h = 40.0$ km; $|c_{ph}^{in}| = 14.7$ m/s; $|c_{pz}^{in}| = 1.6$ m/s; $N_b = 2.1\cdot10^{-2}$ rad/s; $\omega = 2.3\cdot10^{-3}$ rad/s; $\tau_i = 45.5$ min.
Layer c ($h' = 133$ km, $\Delta h = 30$ km): $\lambda_z = 3.0$ km; $\delta = 6.4°$; $|\tan\delta| = 0.11$; $\lambda_h = 27.3$ km; $|c_{ph}^{in}| = 11.0$ m/s; $|c_{pz}^{in}| = 1.2$ m/s; $N_b = 2.3\cdot10^{-2}$ rad/s; $\omega = 2.5\cdot10^{-3}$ rad/s; $\tau_i = 41.9$ min.

It is important that in accordance with Eq. (17), the magnitudes of intrinsic frequency and period can be determined from the values of Brunt-Vaisala frequency (N_b) and angle (δ) between the local vertical and wave propagation vector, only. Calculated from Eq. (17), the internal waves

have the intrinsic periods from 35 to 46 min and intrinsic vertical phase speeds from 1.4 to 2.0 m/s. These values fully correspond to a period of 30 min in the ground-based frame and downward wind speed of 2.0 m/s at a height of 100 km for a model of the polar cap Sporadic-E layers (MacDougall et al., 2000b). It should be noted that because the locations of wind nodes coincide with those for E_s layers, then the intrinsic and ground-based wave periods must be equal each to other. In this case, the intrinsic wave periods τ_i from 35 to 46 min correspond to results obtained in the high-latitude investigations by Kirkwood and Collis (1989), Turunen et al. (1993), Heinselman et al. (1998), MacDougall et al. (2000a,b). Thus, we have developed a new indirect technique for determining the parameters of internal waves responsible for the tilts of sporadic plasma layers at the E region heights. We have shown that the intrinsic wave frequency and period, vertical and horizontal wavelengths, intrinsic vertical and horizontal phase speeds, and other characteristics of IGWs under study can be found using our analysis.

5. Summary

We have used the satellite CHAMP/GPS RO data for studying the high-latitude ionosphere of the Earth. A method for deriving the parameters of ionospheric structures is based upon an analysis of the RO signal variations in the phase path and intensity. This method allows one to estimate the spatial displacement of a plasma layer with respect to the ray perigee, and to determine the layer inclination and height correction values. Assuming that internal gravity waves with the phase-fronts parallel to the ionization layer surfaces are responsible for the tilt angles of sporadic plasma layers, we have developed a new indirect technique for determining the parameters of IGWs linked with the inclined E_s structures. A small-scale internal wave may be modulating initially horizontal E_s layer in height and causing a direction of the plasma density gradient to be rotated and aligned with that of the wave propagation vector $\boldsymbol{k}$. The results of determination of the intrinsic wave frequency and period, vertical and horizontal wavelengths, intrinsic vertical and horizontal phase speeds, and other characteristics of internal waves under study have been presented. The developed technique extends capabilities of the RO method for studying the atmospheres and ionospheres of the Earth and planets.

Acknowledgements

This work was partially supported by the Program 1.7 of the RAS Presidium. The reported study was funded by RFBR according to the research project No. 18-02-00313. We thank the Referees for their valuable suggestions.

References

Arras, C., Wickert, J., Beyerle, G., Heise, S., Schmidt, T., Jacobi, C., 2008. A global climatology of ionospheric irregularities derived from GPS radio occultation. Geophys. Res. Lett. 35, L14809. https://doi.org/10.1029/2008GL03415.

Bernhardt, P.A., 2002. The modulation of sporadic-E layers by Kelvin-Helmholtz billows in the neutral atmosphere. J. Atmos. Sol.-Terr. Phys. 64, 1487–1504.

Bernhardt, P.A., Selcher, C.A., Siefring, C., Wilkens, M., Compton, C., Bust, G., Yamamoto, M., Fukao, S., Takayuki, O., Wakabayashi, M., Mori, H., 2005. Radio tomographic imaging of sporadic-E layers during SEEK-2. Ann. Geophys. 23, 2357–2368. https://doi.org/10.5194/angeo-23-2357-2005.

Bristow, W.A., Watkins, B.J., 1991. Numerical simulation of the formation of thin ionization layers at high latitudes. Geophys. Res. Lett. 18, 404–407.

Bristow, W.A., Watkins, B.J., 1993. Incoherent scatter observations of thin ionization layers at Sondrestrom. J. Atmos. Terr. Phys. 55, 873–894.

Chimonas, G., Axford, W.I., 1968. Vertical movement of temperate-zone sporadic *E* layers. J. Geophys. Res. 73, 111–117.

Chimonas, G., 1971. Enhancement of sporadic **E** by horizontal transport within the layer. J. Geophys. Res. 76, 4578–4586.

Chu, Y.-H., Brahmanandam, P.S., Wang, C.-Y., Ching-Lun, S., Kuong, R.-M., 2011. Coordinated sporadic E layer observations made with Chung-Li 30 MHz radar, ionosonde and FORMOSAT-3/COSMIC satellites. J. Atmos. Sol.-Terr. Phys. 73, 883–894.

Cosgrove, R.B., Tsunoda, R.T., 2002. A direction-dependent instability of sporadic-E layers in the nighttime midlatitude ionosphere. Geophys. Res. Lett. 29 (18), 1864. https://doi.org/10.1029/2002GL014669.

Cosgrove, R.B., Tsunoda, R.T., 2004. Instability of the E-F coupled nighttime midlatitude ionosphere. J. Geophys. Res. 109, A04305. https://doi.org/10.1029/2003JA010243.

Cox, R.M., Plane, J.M.C., 1998. An ion-molecule mechanism for the formation of neutral sporadic Na layers. J. Geophys. Res. 103 (D6), 6349–6359.

Didebulidze, G.G., Lomidze, L.N., 2010. Double atmospheric gravity wave frequency oscillations of sporadic E formed in a horizontal shear flow. Phys. Lett. A 374 (7), 952–969.

Fritts, D.C., Alexander, M.J., 2003. Gravity wave dynamics and effects in the middle atmosphere. Rev. Geophys. 41, 1003. https://doi.org/10.1029/2001RG000106.

Gorbunov, M.E., Gurvich, A.S., Shmakov, A.V., 2002. Back-propagation and radio-holographic methods for investigation of sporadic ionospheric E-layers from Microlab-1 data. Int. J. Remote Sens. 23, 675–685.

Gossard, E.E., Hooke, W.H., 1975. Waves in the Atmosphere. Elsevier Scientific Publishing Co, Amsterdam–Oxford–New York.

Gubenko, V.N., Andreev, V.E., 2003. Radio wave fluctuations and layered structure of the upper region of Venusian clouds from radio occultation data. Cosmic Res. 41 (2), 135–140. https://doi.org/10.1023/A:1023378829327.

Gubenko, V.N., Andreev, V.E., 2007. The identification of the fluctuation effects related to the turbulence and "permanent" layers in the atmosphere of Venus from radio occultation data. Astron. Astrophys. Trans. 26 (6), 507–515. https://doi.org/10.1080/10556790701610399.

Gubenko, V.N., Andreev, V.E., Pavelyev, A.G., 2008a. Detection of layering in the upper cloud layer of Venus northern polar atmosphere observed from radio occultation data. J. Geophys. Res. 113, E03001. https://doi.org/10.1029/2007JE002940.

Gubenko, V.N., Pavelyev, A.G., Andreev, V.E., 2008b. Determination of the intrinsic frequency and other wave parameters from a single vertical temperature or density profile measurement. J. Geophys. Res. 113, D08109. https://doi.org/10.1029/2007JD008920.

Gubenko, V.N., Pavelyev, A.G., Salimzyanov, R.R., Pavelyev, A.A., 2011. Reconstruction of internal gravity wave parameters from radio occultation retrievals of vertical temperature profiles in the Earth's atmosphere. Atmos. Meas. Tech. 4 (10), 2153–2162. https://doi.org/10.5194/amt-4-2153-2011.

Gubenko, V.N., Pavelyev, A.G., Salimzyanov, R.R., Andreev, V.E., 2012. A method for determination of internal gravity wave parameters from a vertical temperature or density profile measurement in the Earth's atmosphere. Cosmic Res. 50 (1), 21–31. https://doi.org/10.1134/S0010952512010029.

Gubenko, V.N., Kirillovich, I.A., Pavelyev, A.G., 2015. Characteristics of internal waves in the Martian atmosphere obtained on the basis of an analysis of vertical temperature profiles of the Mars Global Surveyor mission. Cosmic Res. 53 (2), 133–142. https://doi.org/10.1134/S0010952515020021.

Gubenko, V.N., Kirillovich, I.A., Pavelyev, A.G., Andreev, V.E., 2016a. Detection of saturated internal gravity waves and reconstruction of their characteristics in the Martian atmosphere. Izvestiya Vysshikh Uchebnykh Zavedenii. Fizika 59 (12–2), 46–49, ISSN 0021–3411 (in Russian).

Gubenko, V.N., Kirillovich, I.A., Liou, Y.-A., Pavelyev, A.G., 2016b. Monitoring of internal gravity waves in the Arctic and Antarctic atmosphere. Izvestiya Vysshikh Uchebnykh Zavedenii. Fizika 59 (12–3), 80–85, ISSN 0021–3411 (in Russian).

Haldoupis, C.A., 2011. Tutorial Review on Sporadic E layers. Chapter in book: Aeronomy of the Earth's Atmosphere and Ionosphere. In: Abdu, M.A., Pancheva, D., Bhattacharyya, A. (Eds.) IAGA Special Sopron Book Series 2, 381–394, Springer, Berlin, doi: https://doi.org/10.1007/978-94-007-0326-1-2.

Haldoupis, C., 2012. Midlatitude Sporadic E layers. A typical paradigm of atmosphere–ionosphere coupling. Space Sci. Rev. 168, 441–461.

Heinselman, C.J., Thayer, J.P., Watkins, B.J., 1998. A high-latitude observation of sporadic sodium and sporadic E-layer formation. Geophys. Res. Lett. 25, 3059–3062.

Hunten, D.M., Turco, R.P., Toon, O.B., 1980. Smoke and dust particles of meteoric origin in the mesosphere and stratosphere. J. Atmos. Sci. 37, 1342–1357.

Hysell, D.L., Yamamoto, M., Fukao, S., 2002. Imaging radar observations and theory of type I and type II quasi-periodic echoes. J. Geophys. Res. 107 (A11), 1360. https://doi.org/10.1029/2002JA009292.

Hysell, D.L., Larsen, M.F., Zhou, Q.H., 2004. Common volume coherent and incoherent scatter radar observations of mid-latitude sporadic E-layers and QP echoes. Ann. Geophys. 22, 3277–3290. https://doi.org/10.5194/angeo-22-3277-2004.

Hysell, D.L., Nossa, E., Larsen, M.F., Munro, J., Sulzer, M.P., González, S.A., 2009. Sporadic E layer observations over Arecibo using coherent and incoherent scatter radar: Assessing dynamic stability in the lower thermosphere. J. Geophys. Res. 114, A12303. https://doi.org/10.1029/2009JA014403.

Hines, C.O., 1960. Internal atmospheric gravity waves at ionospheric heights. Can. J. Phys. 38, 1441–1481.

Igarashi, K., Pavelyev, A.G., Hocke, K., Pavelyev, D., Wickert, J., 2001. Observation of wave structures in the upper atmosphere by means of radio holographic analysis of the RO data. Adv. Space Res. 27, 1321–1327.

Kato, S., Reddy, C.A., Matsushita, S., 1970. Possible hydromagnetic coupling between the perturbations of the neutral and ionized atmosphere. J. Geophys. Res. 75, 2540–2550.

Kelley, M.C., 2009. The Earth's Ionosphere: Plasma Physics and Electrodynamics, second ed. Academic Press, San Diego, California, p. 556.

Kirchengast, G., Foelsche, U., Steiner, A. (Eds.), 2004. Occultations for Probing Atmosphere and Climate. Springer, Berlin.

Kirkwood, S., Collis, P.N., 1989. Gravity wave generation of simultaneous auroral sporadic-*E* layers and sudden neutral sodium layers. J. Atmos. Terr. Phys. 51 (4), 259–269.

Kirkwood, S., von Zahn, U., 1991. On the role of auroral electric fields in the formation of low altitude sporadic-E and sudden sodium layers. J. Atmos. Terr. Phys. 53, 389–407.

Kirkwood, S., von Zahn, U., 1993. Formation mechanisms for low altitude Es and their relationship with neutral Fe layers: Results from the METAL campaign. J. Geophys. Res. 98, 21549–21561.

Kirkwood, S., Nilsson, H., 2000. High-latitude sporadic-E and other thin layers – the role of magnetospheric electric fields. Space Sci. Rev. 91, 579–613.

Kliore, A., Cain, D.L., Levy, G.S., Eshleman, V.R., Fjeldbo, G., Drake, F.D., 1965. Occultation experiment: results of the first direct measurement of Mars's atmosphere and ionosphere. Science 149, 1243–1248.

Kunitsyn, V.E., Tereshchenko, E.D., 2003. Ionospheric Tomography. Springer-Verlag, Berlin.

Larsen, M.F., Fukao, S., Yamamoto, M., Tsunoda, R., Igarashi, K., Ono, T., 1998. The SEEK chemical release experiment: Observed neutral wind profile in a region of sporadic-E. Geophys. Res. Lett. 25, 1789–1792.

Larsen, M.F., 2000. A shear instability seeding mechanism for quasiperiodic radar echoes. J. Geophys. Res. 105 (A11), 24931–24940. https://doi.org/10.1029/1999JA000290.

Larsen, M.F., Yamamoto, M., Fukao, S., Tsunoda, R.T., 2005. SEEK 2: Observations of neutral winds, wind shears, and wave structure during a sporadic E/QP event. Ann. Geophys. 23, 2369–2375.

Larsen, M.F., Hysell, D.L., Zhou, Q.H., Smith, S.M., Friedman, J., Bishop, R.L., 2007. Imaging coherent scatter radar, incoherent scatter radar, and optical observations of quasiperiodic structures associated with sporadic E layers. J. Geophys. Res. 112, A06321. https://doi.org/10.1029/2006JA012051.

Lehmacher, G.A., Larsen, M.F., Croskey, C.L., 2015. Observation of electron biteout regions below sporadic E layers at polar latitudes. Ann. Geophys. 33, 371–380. https://doi.org/10.5194/angeo-33-371-2015.

Liou, Y.A., Pavelyev, A.G., 2006. Simultaneous observations of radio wave phase and intensity variations for locating the plasma layers in the ionosphere. Geophys. Res. Lett. 33, L23102. https://doi.org/10.1029/2006GL027112.

Liou, Y.-A., Pavelyev, A.G., Liu, S.-F., Pavelyev, A.A., Yen, N., Huang, C.-Y., Fong, C.-J., 2007. FORMOSAT-3/COSMIC GPS radio occultation mission: preliminary results. IEEE T. Geosci. Remote Sens. 45, 3813–3826.

Liou, Y.A., Pavelyev, A.G., Matyugov, S.S., Yakovlev, O.I., Wickert, J., 2010. Radio Occultation Method for Remote Sensing of the Atmosphere and Ionosphere. Edited by: Liou, Y.A., INTECH, 32000 Vukovar. Croatia, 170, 45 pp., ISBN 978-953-7619-60-2.

MacDougall, J.W., Jayachandran, P.T., Plane, J.M.C., 2000a. Polar cap sporadic-E: part 1, observations. J. Atmos. Sol.-Terr. Phys. 62, 1155–1167.

MacDougall, J.W., Plane, J.M.C., Jayachandran, P.T., 2000b. Polar cap sporadic-E: part 2, modeling. J. Atmos. Sol.-Terr. Phys. 62, 1169–1176.

Malhotra, A., Mathews, J.D., Urbina, J., 2008. Effect of meteor ionization on sporadic-E observed at Jicamarca. Geophys. Res. Lett. 35, L15106. https://doi.org/10.1029/2008GL034661.

Maruyama, T., Fukao, S., Yamamoto, M., 2000. A possible mechanism for echo striation generation of radar backscatter from midlatitude sporadic E. Radio Sci. 35, 1155–1164.

Maruyama, T., Kato, H., Nakamura, M., 2003. Ionospheric effects of the Leonid meteor shower in November 2001 as observed by rapid run ionosondes. J. Geophys. Res. 108 (A8), 1324. https://doi.org/10.1029/2003JA009831.

Maruyama, T., Kato, H., Nakamura, M., 2008. Meteor-induced transient sporadic E as inferred from rapid-run ionosonde observations at midlatitudes. J. Geophys. Res. 113, A09308. https://doi.org/10.1029/2008JA013362.

Mathews, J.D., 1998. Sporadic E: Current views and recent progress. J. Atmos. Sol.-Terr. Phys. 60 (4), 413–435. https://doi.org/10.1016/S1364-6826(97)00043-6.

Nygren, T., Jalonen, L., Oksman, J., Turunen, T., 1984. The role of electric field and neutral wind direction in the formation of sporadic E-layers. J. Atmos. Terr. Phys. 46, 373–381.

Ogawa, T., Takahashi, O., Otsuka, Y., Nozaki, K., Yamamoto, M., Kita, K., 2002. Simultaneous middle and upper atmosphere radar and ionospheric sounder observations of midlatitude E region irregularities and sporadic E layer. J. Geophys. Res. 107 (A10), 1275. https://doi.org/10.1029/2001JA900176.

Otsuka, Y., Shiokawa, K., Ogawa, T., Yokoyama, T., Yamamoto, M., 2009. Spatial relationship of nighttime medium-scale traveling ionospheric disturbances and F region field-aligned irregularities observed with two spaced all-sky airglow imagers and the middle and upper atmosphere radar. J. Geophys. Res. 114, A05302. https://doi.org/10.1029/2008JA013902.

Pavelyev, A.G., Wickert, J., Liou, Y.-A., 2008. Localization of plasma layers in the ionosphere based on observing variations in the amplitude and phase of radiowaves along the satellite-to-satellite path. Radiophys. Quantum Electron. 51, 1–8.

Pavelyev, A.G., Liou, Y.A., Wickert, J., Gubenko, V.N., Pavelyev, A.A., Matyugov, S.S., 2009. New Applications and Advances of the GPS Radio Occultation Technology as Recovered by Analysis of the FORMOSAT-3/COSMIC and CHAMP Data-Base. Chapter in book: New Horizons in Occultation Research: Studies in Atmosphere and Climate. In: Steiner, A., Pirscher, B., Foelsche, U., Kirchengast, G. (Eds.). Springer-Verlag, Berlin, Heidelberg, pp. 165–178, doi: https://doi.org/10.1007/978-3-642-00321_9.

Pavelyev, A.G., Liou, Y.A., Wickert, J., Gavrik, A.L., Lee, C.C., 2009b. Eikonal acceleration technique for studying of the Earth and planetary atmospheres by radio occultation method. Geophys. Res. Lett. 36, L21807. https://doi.org/10.1029/2009GL040979.

Pavelyev, A.G., Liou, Y.-A., Wickert, J., Schmidt, T., Pavelyev, A.A., Matyugov, S.S., 2010. Phase acceleration: a new important parameter in GPS occultation technology. GPS Solutions 14, 3–14. https://doi.org/10.1007/s10291-009-0128-1.

Pavelyev, A.G., Liou, Y.A., Zhang, K., Wang, C.S., Wickert, J., Schmidt, T., Gubenko, V.N., Pavelyev, A.A., Kuleshov, Y., 2012. Identification and localization of layers in the ionosphere using the eikonal and amplitude of radio occultation signals. Atmos. Meas. Tech. 5 (1), 1–16. https://doi.org/10.5194/amt-5-1-2012.

Pavelyev, A.G., Liou, Y.A., Matyugov, S.S., Pavelyev, A.A., Gubenko, V.N., Zhang, K., Kuleshov, Y., 2015. Application of the locality principle to radio occultation studies of the Earth's atmosphere and ionosphere. Atmos. Meas. Tech. 8 (7), 2885–2899. https://doi.org/10.5194/amt-8-2885-2015.

Pezzopane, M., Pignalberi, A., Pietrella, M., 2016. On the solar cycle dependence of the amplitude modulation characterizing the mid-latitude sporadic E layer diurnal periodicity. J. Atmos. Sol.-Terr. Phys. 137, 29–35. https://doi.org/10.1016/j.jastp.2015.11.010.

Pietrella, M., Bianchi, C., 2009. Occurrence of sporadic-E layer over the ionospheric station of Rome: Analysis of data for thirty-two years. Adv. Space Res. 44 (1), 72–81. https://doi.org/10.1016/j.asr.2009.03.006.

Pietrella, M., Pezzopane, M., Bianchi, C., 2014. A comparative sporadic-E layer study between two mid-latitude ionospheric stations. Adv. Space Res. 54 (2), 150–160. https://doi.org/10.1016/j.asr.2014.03.019.

Roddy, P.A., Earle, G.D., Swenson, C.M., Carlson, C.G., Bullett, T.W., 2004. Relative concentrations of molecular and metallic ions in midlatitude intermediate and sporadic-E layers. Geophys. Res. Lett. 31, L19807. https://doi.org/10.1029/2004GL020604.

Saito, S., Yamamoto, M., Hashiguchi, H., Maegawa, A., 2006. Observation of three-dimensional structures of quasi-periodic echoes associated with mid-latitude sporadic-E layers by MU radar ultra-multi-channel system. Geophys. Res. Lett. 33, L14109. https://doi.org/10.1029/2005GL025526.

Sokolovskiy, S.V., Schreiner, W., Rocken, C., Hunt, D., 2002. Detection of high-altitude ionospheric irregularities with GPS/MET. Geophys. Res. Lett. 29, 621–625.

Tsunoda, R.T., Cosgrove, R.B., 2001. Coupled electrodynamics in the nighttime midlatitude ionosphere. Geophys. Res. Lett. 28, 4171–4174.

Tsunoda, R.T., Fukao, S., Yamamoto, M., 1994. On the origin of quasiperiodic radar backscatter from midlatitude sporadic E. Radio Sci. 29, 349–366.

Turunen, T., Nygren, T., Huuskonen, A., 1993. Nocturnal high-latitude E-region in winter during extremely quiet conditions. J. Atmos. Terr. Phys. 55, 783–795.

Vorob'ev, V.V., Gurvich, A.S., Kan, V., Sokolovskiy, S.V., Fedorova, O. V., Shmakov, A.V., 1997. The structure of the ionosphere from the GPS-"Microlab-1" radio occultation data: Preliminary results. Issled. Zemli Kosm. 4, 74–83 (in Russian).

Ware, R., Exner, M., Feng, D., Gorbunov, M., Hardy, K., Herman, B., Kuo, Y.-H., Meehan, T., Melbourn, W., Rocken, C., Schreiner, W., Sokolovskiy, S., Solheim, F., Zou, X., Anthes, R., Businger, S., Trenberth, K., 1996. GPS soundings of the atmosphere from low earth orbit: Preliminary results. B. Am. Meteorol. Soc. 77, 19–40.

Watson, C., Jayachandran, P.T., Spanswick, E., Donovan, E.F., Danskin, D.W., 2011. GPS TEC technique for observation of the evolution of substorm particle precipitation. J. Geophys. Res. 116, A00I90. https://doi.org/10.1029/2010JA015732.

Watson, C., Jayachandran, P.T., MacDougall, J.W., 2016. Characteristics of GPS TEC variations in the polar cap ionosphere. J. Geophys. Res. 121, 4748–4768. https://doi.org/10.1002/2015JA022275.

Whitehead, J.D., 1971. Ionization disturbances caused by gravity waves in the presence of an electrostatic field and background wind. J. Geophys. Res. 76, 238–241.

Whitehead, J.D., 1972. Winds in *E* region. Radio Sci. 7, 403–404.

Whitehead, J.D., 1989. Recent work on midlatitude and equatorial sporadic E. J. Atmos. Terr. Phys. 51, 401–424. https://doi.org/10.1016/0021-9169(89)90122-0.

Wickert, J., Pavelyev, A.G., Liou, Y.A., Schmidt, T., Reigber, Ch., Igarashi, K., Pavelyev, A.A., Matyugov, S., 2004. Amplitude scintillations in GPS signals as a possible indicator of ionospheric structures. Geophys. Res. Lett. 31, L24801. https://doi.org/10.1029/2004GL020607.

Woodman, R.F., Yamamoto, M., Fukao, S., 1991. Gravity wave modulation of gradient drift instabilities in mid-latitude sporadic E irregularities. Geophys. Res. Lett. 18, 1197–1200. https://doi.org/10.1029/91GL01159.

Wu, D.L., Ao, C.O., Hajj, G.A., de la Torre Juarez, M., Mannucci, A.J., 2005. Sporadic *E* morphology from GPS-CHAMP radio occultations. J. Geophys. Res. 110, A01306. https://doi.org/10.1029/2004JA010701.

Yakovlev, O.I., Matyugov, S.S., Gubenko, V.N., 1991. Venera-15 and -16 middle atmosphere profiles from radio occultations: Polar and near-polar atmosphere of Venus. Icarus 94 (2), 493–510. https://doi.org/10.1016/0019-1035(91)90243-M.

Yakovlev, O.I., Pavelyev, A.G., Matyugov, S.S., 2010. Radio Occultation Monitoring of the Atmosphere and Ionosphere. URSS Edition, Moscow, 206 pp., ISBN 978-5-397-01227-0 (in Russian).

Yamamoto, M., Fukao, S., Woodman, R.F., Ogawa, T., Tsuda, T., Kato, K., 1991. Mid-latitude *E* region field-aligned irregularities observed with the MU radar. J. Geophys. Res.-Space. 96, 15943–15949.

Yamamoto, M., Fukao, S., Ogawa, T., Tsuda, T., Kato, S., 1992. A morphological study of mid-latitude *E*-region field-aligned irregularities observed with the MU radar. J. Atmos. Sol.-Terr. Phys. 54, 769–777.

Yamamoto, M., Fukao, S., Tsunoda, R.T., Pfaff, R., Hayakawa, H., 2005. SEEK-2 (Sporadic-*E* Experiment over Kyushu 2) – project outline, and significance. Ann. Geophys. 23, 2295–2305. https://doi.org/10.5194/angeo-23-2295-2005.

Yeh, W.-H., Liu, J.-Y., Huang, C.-Y., Chen, S.-P., 2014. Explanation of the sporadic-*E* layer formation by comparing FORMOSAT-3/COSMIC data with meteor and wind shear information. J. Geophys. Res. 119, 4568–4579. https://doi.org/10.1002/2013JD020798.

Yokoyama, T., Yamamoto, M., Fukao, S., Cosgrove, R.B., 2004. Three-dimensional simulation on generation of polarization electric field in the midlatitude E-region ionosphere. J. Geophys. Res. 109, A01309. https://doi.org/10.1029/2003JA010238.

Yokoyama, T., Yamamoto, M., Fukao, S., Takahashi, T., Tanaka, M., 2005. Numerical simulation of mid-latitude ionospheric *E*-region based on SEEK and SEEK-2 observations. Ann. Geophys. 23 (7), 2377–2384.

Yokoyama, T., Hysell, D.L., Otsuka, Y., Yamamoto, M., 2009. Three-dimensional simulation of the coupled Perkins and Es-layer instabilities in the nighttime midlatitude ionosphere. J. Geophys. Res. 114, A03308. https://doi.org/10.1029/2008JA013789.

Yue, X., Schreiner, W.S., Zeng, Z., Kuo, Y.-H., Xue, X., 2015. Case study on complex sporadic E layers observed by GPS radio occultations. Atmos. Meas. Tech. 8, 225–236. https://doi.org/10.5194/amt-8-225-2015.

Zeng, Z., Sokolovskiy, S., 2010. Effect of sporadic E cloud on GPS radio occultation signal. Geophys. Res. Lett. 37, L18817. https://doi.org/10.1029/2010GL044561.